Food Chemistry 526 (2026) 150774

Contents lists available at ScienceDirect

Food Chemistry

journal homepage: www.elsevier.com/locate/foodchem

Impact of genetic modifications in starch biosynthesis on 3D printing performance of rice starches

Yaqi Hu [a,1], Ziliang Qin [b,1], Li Ding [b], Xiaoning Liu [b], Xingxun Liu [c], Deyong Zhu [d], Jacob Judas Kain Kirkensgaard [e,f], Tomasz Pawel Czaja [f], Sheng Chen [b,i], Andreas Blennow [g], Jiyu Yang [b], Jinsong Bao [a,*], Yuyue Zhong [b,h,i,**]

[a] Institute of Nuclear Agricultural Sciences, College of Agriculture and Biotechnology, Institute of Hainan, Zhejiang University, Hangzhou 310058, China
[b] Department of Food Science and Nutrition, The Hong Kong Polytechnic University, Hung Hom, Kowloon, Hong Kong, China
[c] Lab of Food Soft Matter Structure and Advanced Manufacturing, College of Food Science and Engineering, Nanjing University of Finance and Economics, Nanjing 210023, China
[d] Department of Biology, University of Copenhagen, Denmark
[e] Niels Bohr Institute, University of Copenhagen, DK-2100 Copenhagen Ø, Denmark
[f] Department of Food Science, University of Copenhagen, DK-1958 Frederiksberg C, Denmark
[g] Department of Plant and Environmental Sciences, Faculty of Science, University of Copenhagen, Denmark
[h] Research Institute for Microbiology, The Hong Kong Polytechnic University, Hung Hom, Kowloon, Hong Kong SAR
[i] Food Nutrition and Health Research Centre, The Hong Kong Polytechnic University Shaoxing Technology and Innovation Research Institute, Zhejiang, 312000, China

ARTICLE INFO

Keywords:
Rice starch
Amylopectin chain length
3D printing
Genetic modification
Starch gels

ABSTRACT

Starch gels with favorable rheological properties are promising for 3D printing, but native starch often requires modification, and traditional physical or chemical methods may pose safety and food applicability concerns. In this study, we investigated the effects of gene modification in starch biosynthesis on gel microstructure, rheological behavior, and 3D printing performance of rice starch. Six rice starch samples with varying genotypes and molecular structures were selected to prepare starch gels retrograded for 1 h, 1 day, and 7 days. Knockout of *starch branching enzyme IIb* (*BEIIb*) increased amylose content (>30%), resulting in starch gels with smaller pore area/fraction, and correlation length (~20–40 Å) and structural radii of the semicrystalline units, and faster recrystallization, but lower yield stress (<20 Pa) and shear recovery (~30%–60%) during extended retrogradation, yielding optimal mid-term but limited long-term printability compared to the other three starch samples. In samples with intact *BEIIb*, the $SSIIa^{TT}$ genotype increased fa chain content (27%–28%), thereby improving pore fraction, correlation length (~35–55 Å) and structural radii, delaying B-type crystallization, and presenting the best initial and long-term printability. In contrast, the $SSIIa^{GC}$ genotype had higher fb1 chain content (52%), yield stress (~60–120 Pa), and consistency index (~40–85 Pa·sn), but low pore area/fraction values, supporting good mid-term printability. These results indicate that both amylose content and amylopectin fine structure significantly affect starch printability. This genetic approach offers a sustainable, precise, and cost-effective solution for optimizing starch materials for 3D printing.

1. Introduction

Rice (*Oryza sativa* L.) is a major staple crop, widely consumed as food and utilized across various industries. In the food sector, three-dimensional (3D) printing is an emerging technology that offers significant advantages over traditional manufacturing methods, including the ability to fabricate complex shapes, personalize nutritional content, and broaden the range of usable food ingredients. Starch, a renewable and cost-effective biopolymer, is considered an ideal material for 3D food printing due to its capacity to form gels with favorable rheological and mechanical properties (Cisneros, Zevillanos, & Cisneros-Zevallos, 2009; Moo-Huchin et al., 2015; Zeeman, Kossmann, & Smith, 2010). Upon

* Corresponding author.
** Corresponding author.
E-mail addresses: jsbao@zju.edu.cn (J. Bao), yuyuezhong93@163.com (Y. Zhong).
[1] The authors contributed equally.

https://doi.org/10.1016/j.foodchem.2026.150774
Received 27 October 2025; Received in revised form 15 March 2026; Accepted 11 August 2026
Available online 12 August 2026
0308-8146/© 2026 Elsevier Ltd. All rights are reserved, including those for text and data mining, AI training, and similar technologies.

heating, starch undergoes gelatinization, resulting in the formation of starch gels that retain their shape and stability after printing, thereby making starch highly suitable for precise 3D food printing applications (Rong et al., 2022). Rice starch is particularly attractive for extrusion-based 3D food printing because its granules generally show relatively small size, low lipid and protein interference, and a tunable molecular architecture, including specific amylose content and amylopectin chain-length distributions that profoundly influence gelatinization, pasting and gel rheology(Bhardwaj & Saini, 2025; Jain, Winuprasith, & Suphantharika, 2019; Wani et al., 2013). In rice starch, amylopectin with a higher proportion of short chains (fa: DP 6–12 and fab1: DP 13–24) is associated with lower gelatinization temperatures and a less ordered crystalline region, whereas longer amylopectin chains contribute to stronger inter-chain associations and higher gel strength (Fei, Han, Yu, Gong, & Jing, 2023; Li & Gong, 2020). Variations in amylose chain-length distribution have been shown to affect the gelatinization temperature range and retrogradation behavior of rice starches, with medium-length amylose chains correlated with narrower gelatinization ranges and enhanced gel network formation (Li, Hu, & Li, 2021). In addition, rice starch can form smooth and homogeneous pastes after thermal treatment, which is beneficial for continuous extrusion and fine filament deposition. These structural and processing features make rice starch a suitable model system for investigating how starch molecular architecture governs 3D printability. (Feng, Wang, Li, Zhou, & Meng, 2018; Y. Liu et al., 2020; Punia, Sandhu, Dhull, & Kaur, 2019; Zhang et al., 2020).

For extrusion-based 3D food printing, material printability is mainly governed by a balance between flowability during extrusion and stability after deposition (Chen, Zhang, Sun, & Phuhongsung, 2022; Qin et al., 2025; Zeng, Chen, Chen, & Zheng, 2021). Rheological parameters such as yield stress, apparent viscosity, shear-thinning behavior, viscoelasticity, and structural recovery are therefore key determinants of printing performance (Li, Liu, & Li, 2016; Sweeney, Campbell, Hanson, Pantoya, & Christopher, 2017). In rice starch gels, these properties are closely associated with molecular composition and chain architecture. Amylose contributes to intermolecular association, gel firmness, and retrogradation, whereas amylopectin fine structure, especially the relative abundance of short and intermediate chains, affects molecular mobility, water retention, and network recovery after shear (Li et al., 2021). In rice starch, these effects are especially relevant because naturally occurring or breeding-derived variation in starch biosynthetic genes can cause substantial changes in both amylose content and amylopectin chain-length distribution (Hu et al., 2025; Miura et al., 2018; Okpala, Aloryi, An, He, & Tang, 2022). Such differences are expected to influence not only gelatinization and gel structure, but also extrusion behavior, layer stacking, and printing fidelity during storage. However, current studies on starch-based 3D printing have focused mainly on post-harvest modifications, such as hydrothermal treatment, chemical/enzymatic modification, or the addition of hydrocolloids, while much less attention has been paid to tailoring printability through intrinsic starch biosynthesis (Chen, Zhang, et al., 2022; Qin et al., 2025).

Compared with traditional post-harvest modification, genetic regulation of starch structure offers several advantages, including source-level control, reduced downstream processing, and potentially improved reproducibility. However, this strategy also has limitations: breeding or genetic manipulation is time-consuming, requires specialized germplasm resources and technical expertise, and may face regulatory or consumer acceptance challenges depending on the production route and application scenario. Nevertheless, it provides a valuable approach for revealing structure–property relationships and for developing starch materials with targeted functionality. In our previous research, the indica rice varieties Longtefu B (LTF B, *SSIIa*^{TT}*/BEIIb*) and BP577 (*SSIIa*^{GC}*/be2b*) with different genotypes of *starch synthase IIa* (*SSIIa*) and *starch branching enzyme IIb* (*BEIIb*) were used as parental lines. Through molecular marker-assisted cross breeding, we developed recombinant inbred lines (RILs) harboring diverse alleles (Hu et al., 2023). Significant differences in starch structure were observed among these materials, which are hypothesized to result in notable variations in the properties of 3D-printed products. Therefore, the objective of this study was to investigate how breeding-derived differences in *BEIIb* and *SSIIa* related starch structure affect gel microstructure, rheological behavior, and 3D printing performance of rice starches during retrogradation, thereby establishing source-level structure–property–printability relationships. This provides new evidence that molecular marker-assisted breeding can serve as a source-oriented strategy to develop starches with improved and more predictable printing functionality.

2. Material and methods

2.1. Materials

Six rice starches with varying amylose contents (ACs) and chain length distributions (CLDs) were selected in this study (Table S1). These starches were extracted from the indica rice cultivar Longtefu B (LTFB), the amylose extender (ae) mutant BP577, and four additional varieties with distinct phenotypes derived from their crosses. Apparent AC (AAC) values and CLD characteristics of these rice materials were determined in our previous study using the same genetic materials and analytical procedures (Hu et al., 2023), and are summarized in Table S1 to support interpretation of their gel and printing behavior. Among the selected samples, BP577, BL02, and BL03, having *SSIIa*^{GC}*/be2b*, *SSIIa*^{GC}*/be2b* and *SSIIa*^{TT}*/be2b* genotype, exhibited AACs of 33.16%, 33.84%, and 32.94%, respectively, and were therefore classified as ultra-high-amylose-content (UHAC) rice starches. In contrast, LTFB, BL06, and BL10, with *SSIIa*^{TT}*/BE2b*, *SSIIa*^{GC}*/BE2b*, and *SSIIa*^{TT}*/BE2b*, had significantly lower AACs compared to UHAC rice starches (Table S1). Their AAC values were 26.85%, 28.26%, and 27.18%, respectively, and thus categorized as high-amylose-content (HAC) rice starches (Bao, Shen, Sun, & Corke, 2006; Wani et al., 2012).

The study was conducted using a completely randomized design with two replications at the Zhejiang University farm in Hangzhou, China. Mature seeds, harvested in late September, were used for starch extraction from rice flour following the methods as reported (Syahariza, Li, & Hasjim, 2010). The total starch content of all samples was determined using the Megazyme total starch assay kit (Megazyme Int. Ireland Ltd., Wicklow, Ireland), and results confirmed that the starch content in all samples exceeded 95%.

2.2. Sample preparation

A measured amount of rice starch was added to distilled water to prepare a 6% (w/w) suspension. To ensure complete gelatinization of all starch samples under a standardized condition, each 6% (w/w) starch suspension was heated in an oil bath at 130 °C for 30 min with continuous magnetic stirring. This relatively high temperature was selected because some samples with elevated amylose content required more intensive heating to achieve complete gelatinization (He, Qiu, Liao, Sui, & Corke, 2018). After gelatinization, the mixture was cooled to approximately 80 °C. The storage times of 1 h, 1 d, and 7 d were selected to represent early, intermediate, and prolonged retrogradation stages of rice starch gels during refrigerated storage (Li, 2024; Outrequin, Gamonpilas, Siriwatwechakul, & Sreearunothai, 2023; Xiao et al., 2022). In this study, these time points were used operationally to compare short-term changes in printability within the same starch system, rather than to define universal printability categories for all food inks.

2.3. Scanning electron microscopy (SEM)

Starch gels retrograded for different durations were rapidly frozen in liquid nitrogen. The samples were then lyophilized for 48 h, fixed, and sputter-coated with gold. The morphology of the starch gel network

structure was examined using field emission scanning electron microscopy (FE-SEM; Quanta 200, FEI, Hillsboro, USA). The pore morphology of the starch gels network structure was analyzed using MIPAR software (MIPAR Image Analysis Inc., USA). Representative SEM images were subjected to grayscale thresholding and segmentation to identify pore regions, after which pore area, pore fraction, equivalent diameter, nearest-neighbor distance, average neighbor distance, and eccentricity were calculated from the binarized images using the same analysis settings for all samples.

2.4. Small-angle X-ray scattering (SAXS)

The microstructure of starch gels was analyzed using a Nano-InXider instrument (Xenocs, Grenoble) equipped with a 100 XL+ microfocus sealed X-ray tube (Rigaku, The Woodlands, Texas, USA). This X-ray tube provided Cu-Kα radiation with a wavelength of 1.54 Å and a 2D Pilatus detector (Dectris Ltd., Baden, Switzerland). The gel samples were loaded into quartz capillaries with a diameter of 1.5 mm, and measurements were conducted for 15 min. Scattering backgrounds from air and water were subtracted from the raw small-angle X-ray scattering (SAXS) data. The SAXS data were then fitted using the Gelgel-fit equation to determine the correlation lengths between adjacent units and the structural radii of individual semi-crystalline units (Putaux, Buleon, & Chanzy, 2000) using the following equation.

$$I(Q) \approx \frac{I_L(0)}{\left(1+[(D+1)/3]Q2\xi^2\right)^{D/2}} + I_G(0) \bullet exp\left(-Q^2R_g^2/3\right) + B$$

2.5. Wide angle X-ray scattering (WAXS)

The crystalline structure of the starch gels was analyzed using a SAXS Lab instrument (Xenocs Nano-inXider, Copenhagen, Denmark). Radially averaged intensity (I) was recorded over a scattering angle (2θ) range of 5° to 30°, under operating conditions of 40 mA current, 40 kV voltage, and Cu-Kα radiation with a wavelength of 0.1542 nm.

2.6. Low-field nuclear magnetic resonance (LF-NMR)

To analyze the distribution and mobility of water during the retrogradation process of starch gels, LF-NMR measurements were performed using an MQR Spectro-P spectrometer (Oxford Instruments, Oxfordshire, UK). The pulse parameters were set according to the method described by Wang et al. (2022). The relaxation times (T2n) and their corresponding signal components (M2n) were recorded.

2.7. Rheological measurements

The rheological behavior of starch gels was characterized using a rheometer (DHR-2, TA Instruments, New Castle, DE, USA) equipped with a plate–plate geometry (40 mm diameter, 0.1 mm gap). Samples were equilibrated at 25 °C for 2 min prior to measurement. Rheological properties relevant to both the extrusion and recovery stages were assessed following the procedure described by Liu et al. (2019), with minor modifications. Yield stress was determined using oscillatory stress sweep mode at 1 Hz, with stress ranging from 1 to 1000 Pa at 25 °C. Shear viscosity was measured in flow ramp mode, with the shear rate increasing from 0.01 to 100 s^{-1} at 25 °C. Rotational recovery tests were conducted to evaluate the shear recoverability of the starch hydrogels at 25 °C by applying a low shear rate of 1 s^{-1} for 180 s, followed by a high shear rate of 100 s^{-1} for 120 s, and then returning to a low shear rate of 1 s^{-1} for 180 s. Shear recoverability was calculated as the percentage of viscosity obtained during the first 30 s of the third step (after exposure to the high shear rate), relative to the average viscosity measured in the first step (Achayuthakan & Suphantharika, 2008). Frequency sweep analysis was performed at 25 °C with an angular frequency range of 1 to 100 rad/s at a constant strain of 1%, within the linear viscoelastic region (LVR).

2.8. 3D printing process

A compression-based bioprinter (CELLINK BIO X, Sweden) was used to evaluate the printability of the starch gels (Fig. 1C). Multi-layered structures were designed (Fig. 1A for pattern dimensions), and stereolithography (STL) files were generated accordingly. These files were converted into G-code using Heartware software (Cellink) and printed onto plastic Petri dishes (Merck, Germany). All printing processes were performed at room temperature (25 °C). A sterile, 22-gauge high-precision blunt needle (Cellink, Sweden) was attached to a 3-mL plastic cartridge for printing (Fig. 1D). Each syringe was loaded with 2 mL of sample per test. The minimum pressure required for continuous extrusion was selected, with the nozzle speed set to 6.0 mm/s, the infill density at 100%, and the needle-to-print surface distance optimized to ensure that the extrusion front was aligned with the needle tip. The interior of each pattern was filled using a grid infill, and all samples were printed in three layers (Fig. 1B). Printing performance was evaluated based on four criteria: extrusion continuity, edge definition, internal filling uniformity, and shape retention after printing. The printed constructs were visually compared across samples and storage times under the same printing conditions. A higher printing quality was assigned to samples that showed continuous filament formation, clear edges, uniform grid filling, and minimal collapse or spreading after deposition.

2.9. Statistical analysis

Each test was performed in at least two replicates. The Analysis of Variance (ANOVA), along with Tukey's range test, was executed using SAS software (version 8, from SAS Institute Inc., Cary, NC, USA). Additionally, Pearson correlation analysis was carried out utilizing the Origin64 software (version 2022, OriginLab, Mass, USA).

3. Results

3.1. Micromorphology of starch gels

In this study, six starch samples were selected, including two parental lines (BP577 and LTFB) and four hybrid varieties (BL02, BL03, BL06, and BL10). These samples were retrograded for 1 h, 1 day, and 7 days, and then subjected to 3D printing experiments. SEM images (Fig. 2A) indicated that all retrograded starch gels after freeze-drying presented porous structures, varying among rice varieties. To further characterize their porous structures, the characteristic pore regions of the starch gels were then identified (Fig. S1), and parameters such as pore area (Fig. 2B), pore fraction (Fig. 2C), equivalent diameter (Fig. S2A), nearest neighbor distance (Fig. S2B), average neighbor distance (Fig. S2C), and eccentricity (Fig. S2D) were calculated. The results indicated that all starch gels exhibited a general decreasing trend in the area, equivalent diameter, nearest neighbor distance, and average neighbor distance as retrogradation time increased, with LTFB having increases from 1 day to 7 days. LTFB and BL10 further showed an increasing pore fraction with prolonged retrogradation, opposite to the decreasing trends of other samples, indicating that lower AAC increased the pore fraction.

3.2. Microstructure of starch gels

SAXS is particularly well-suited for investigating microstructures of starch gels, as it provides detailed information on the nanoscale structure of materials, including the arrangement of crystalline and amorphous regions. Previous studies have shown that, during retrogradation, amylose molecules form parallel- and antiparallel-stranded double helices through both intermolecular and intramolecular interactions (Jane & Robyt, 1984). These double helices subsequently aggregate into

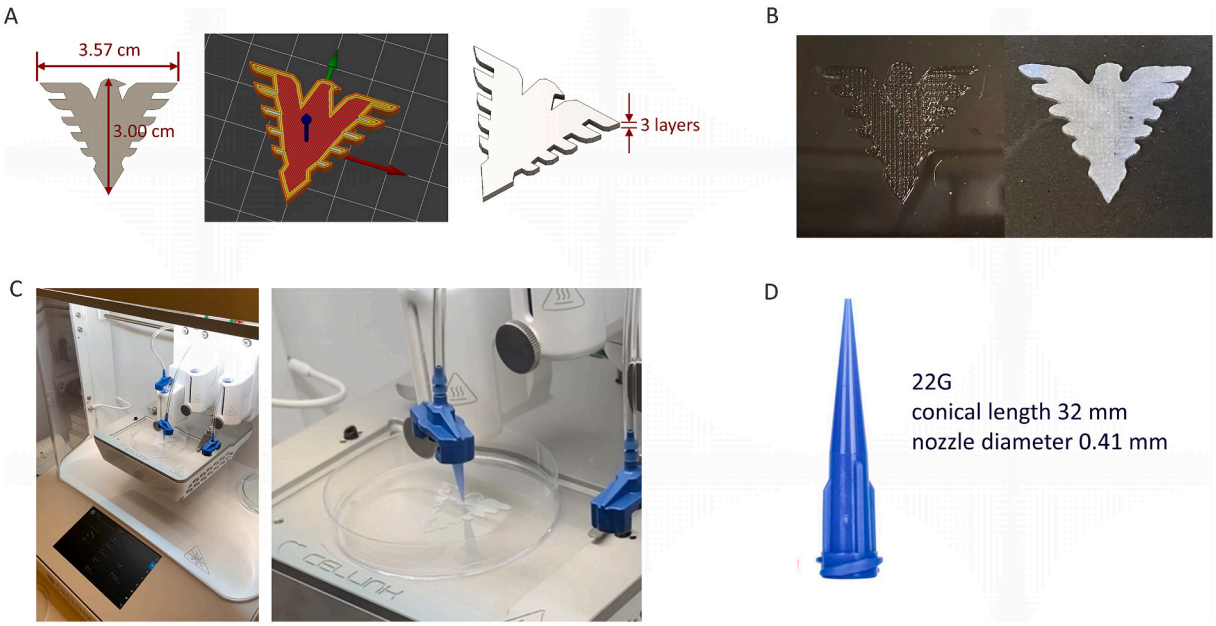


Fig. 1. 3D printing process and design of starch-based products: A) model design and layer structure, B) printed model results, C) 3D printer setup and printing process, D) nozzle specifications.

semicrystalline units, which randomly assemble into a network structure, with more loosely organized chains present between the units (Müller et al., 1995; Putaux et al., 2000).

To quantify these microstructural changes, the SAXS data were fitted using the Gel-fit equation (Fig. S3), which enabled the calculation of correlation lengths between adjacent units and the structural radii (rg) of individual semicrystalline units (Fig. 3). As shown in Fig. 3A, the correlation length of all samples gradually decreased with increasing retrogradation time, although each sample exhibited a distinct trend. Notably, LTFB, BL06 and BL10 had higher correlation lengths than other samples, indicating higher amylose content enhanced the compactness of crystals, thereby decreasing the correlation length. For rg as shown in Fig. 3B, LTFB and BL10 exhibited a general increase trend in rg with prolonged retrogradation time, consistent with the pore fraction data (Fig. 2C).

3.3. Crystalline structure of starch gels

XRD analysis was employed to investigate crystalline structures of starch gels during the retrogradation process (Fig. 4). As shown in Fig. 4A, all starch gels retrograded for 1 h exhibited low retrogradation degree, with BP577, BL02, and BL03 displaying higher intensities of diffraction peaks at 5° and 17°, indicative of the higher amount of B-type crystals generated by starch retrogradation for these UHAC samples. In addition, weak peaks at 14° and 20° for starch gels are likely V-type crystals formed by amylose and endogenous lipids (Gao, Zhang, Qiu, Fu, & Huang, 2020; Liang, Wang, Ma, & Tian, 2024). LTFB, BL06 and BL10 with lower amylose contents showed less pronounced B-type diffraction patterns after 1 h of retrogradation, indicating slower or weaker starch retrogradation. In Fig. 4B (1 day) and Fig. 4C (7 day), the B-type diffraction peaks at 5° and 17° for BP577, BL02, and BL03 showed increased intensities. In addition, new B-type peaks at 22° and 24° appeared, further indicating increasing B-type crystallinity with prolong retrogradation time (Lin, Huang, Zhang, Liu, & Wei, 2020; Ma, Zhu, Wang, Wang, & Wang, 2019). Among HAC starch samples, BL06 exhibited B-type peaks after 1 day of retrogradation, while LTFB and BL10, however, show a less significant change in their diffraction patterns, and weak peaks at 5° and 17° were observed at 7 days. Overall, LTFB and BL10 exhibited slower recrystallization during the retrogradation process, whereas the other four samples, particularly BP577 having the highest AAC, demonstrated faster and more pronounced retrogradation. These observations are consistent with the respective AAC values of the samples.

3.4. Low-field NMR of starch gels

LF-NMR was employed to monitor the changes in water mobility and distributions within starch gels (Fig. 5). These gels exhibited two distinct relaxation populations, with T21 and T22 representing the relaxation times of bound water and free water, respectively (Li et al., 2025; Shi, Wen, Geng, Zhan, & Liu, 2024). A smaller T2 value indicates reduced water mobility and tighter binding (Cheng et al., 2024). M21 and M22 represent the peak areas of bound water and free water, respectively, reflecting their proportions in the total water content (Gao, Sun, Zhao, Wang, & Hou, 2024; Liu, Zhang, Bhandari, & Yang, 2018). For T21 and M21, LTFB and BL10 remained relatively stable over time, whereas the other four samples (BP577, BL02, BL03, and BL06) exhibited increases in these parameters as retrogradation progressed. Additionally, LTFB and BL10 showed only a slight increase in T22 and remained stable in M22, in contrast to the other four samples. These results indicate that the water distribution in LTFB and BL10 did not change significantly during retrogradation. In contrast, BP577, BL02, BL03, and BL06 displayed greater mobility of bound and free water, as well as a higher content of bound water as retrogradation advanced. This suggests that, in these samples, water became more tightly bound within the gel network over time.

3.5. Yield stress of starch gels

Yield stress (flow stress) is critical to the extrudability of ink, as it directly relates to the minimum force required to initiate ink flow (Li et al., 2016; Paxton et al., 2017). During extrusion processes, a low yield stress is highly desirable because extrusion is not continuous and has frequently starts and stops during printing. A high yield stress requires the printer to exert a greater force to exceed the yield threshold (Lewis, 2006). The yield stress of starch gels was determined as the cross-over point where the storage modulus (G') equals the loss modulus (G'') (Fig. 6A) (Wilson, Cross, Peak, & Gaharwar, 2017). The yield stress

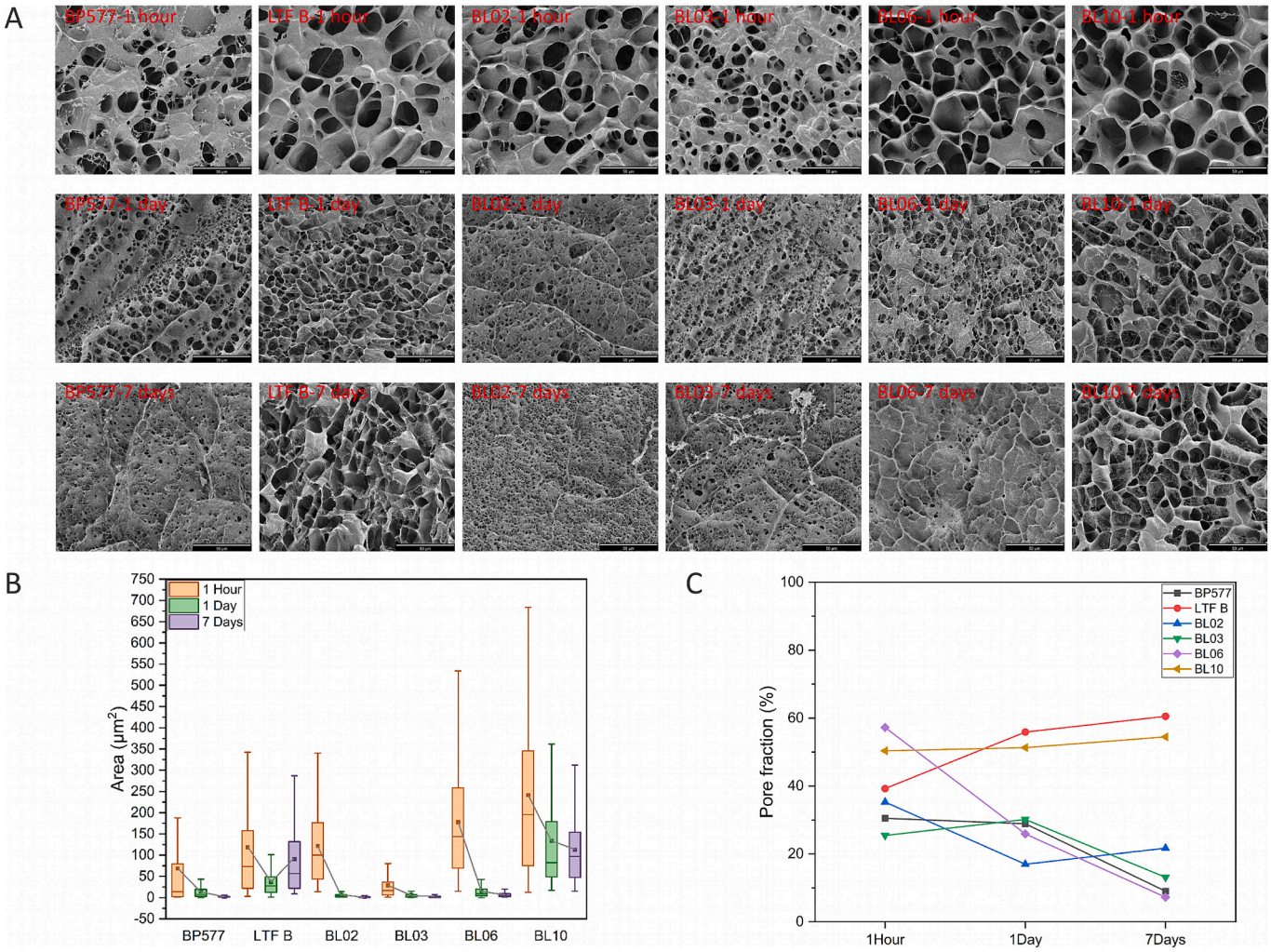


Fig. 2. Scanning electron microscopy (SEM) micrographs and the feature area parameters of different starch hydrogels retrograded for 1 h, 1 day, and 7 days. (A) SEM images of starch hydrogels. (B)Areas of pores. (C)Pore fraction of hydrogels.

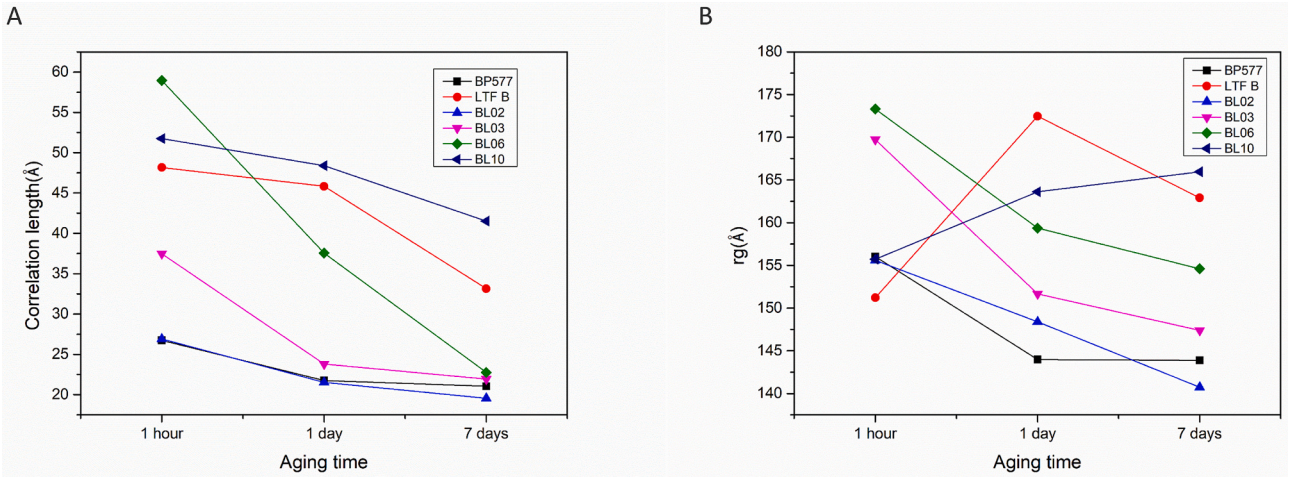


Fig. 3. Correlation length and structural radii (rg) of different starch hydrogels retrograded for 1 h, 1 day, and 7 days. (A) Correlation length. (B) Structural radii (rg).

of starch gels retrograded for 1 h, 1 day, and 7 days is presented in Fig. 6B. Across all six starch samples, yield stress generally exhibited a decreasing trend with increasing retrogradation time. Specifically, BP577, BL02, BL03, and BL06 reached their lowest yield stress on day 1, followed by a partial recovery on day 7. In contrast, LTFB had decreased yield stress and then remained stable, while BL10 showed a continuous decrease in yield stress. Notably, UHAC starch samples (BP577, BL02, and BL03) displayed significantly lower yield stress compared to HAC

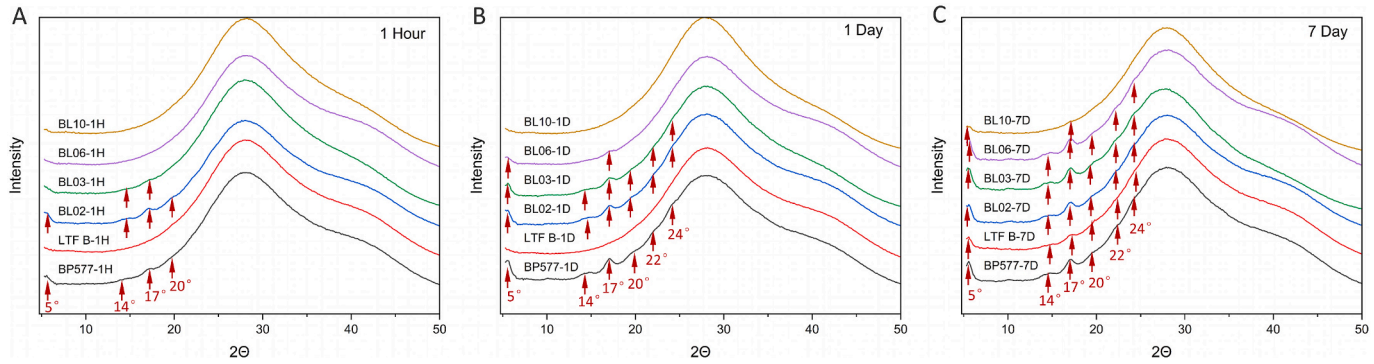


Fig. 4. Wide angle X-ray scattering (WAXS) spectra of different rice starch hydrogels retrograded for 1 h (A), 1 day (B), and 7 days (C).

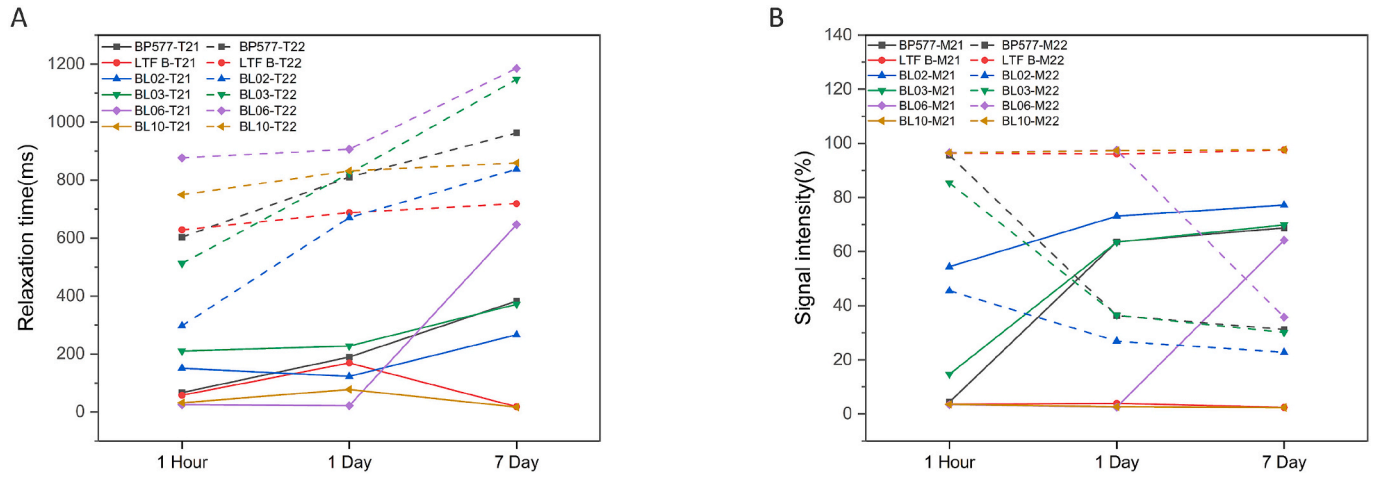


Fig. 5. Transverse relaxation properties of different starch hydrogels retrograded for 1 h, 1 day, and 7 days. (A) Transverse relaxation time (T2), T21: the relaxation times of bound water relaxation peaks, T22: the relaxation times of free water relaxation peaks. (B) Peak areas (M2), M21: the peak areas of bound water relaxation peaks, M22: the peak areas of free water relaxation peaks.

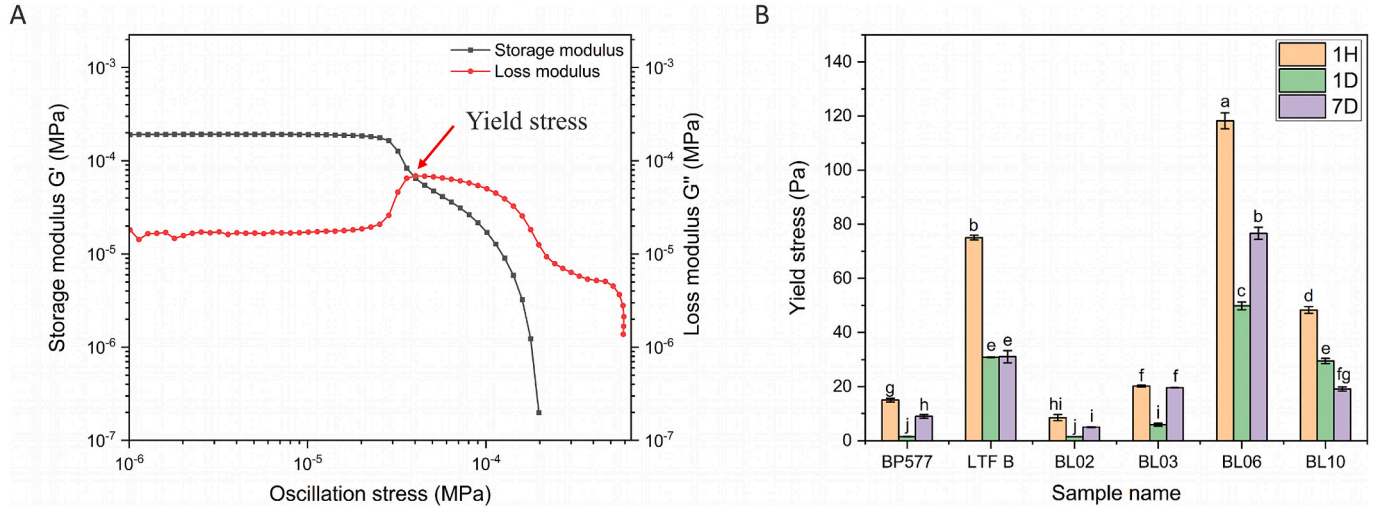


Fig. 6. Yield stress of rice starch hydrogels. (A) Illustrative example of yield stress for the LTFB starch hydrogel retrograded for one day. The yield stress has been determined as the cross-over point where elastic modulus (G′) equals to viscous modulus (G″). (B) Yield stress of different starch hydrogels retrograded for 1 h, 1 day, and 7 days.

samples (LTFB, BL06, and BL10), suggesting that higher AAC enhances the extrusion properties of starch gels.

3.6. *Shear-thinning behavior of starch gels*

After overcoming the yield stress, the pressure required to maintain a continuous flow of starch gels depends on their viscosity and shear-

thinning behavior. The shear-thinning behavior of starch gels can be quantified by fitting the viscosity profiles (Fig. S4) to the power-law equation. The coefficients K and n (Fig. 7) obtained from this equation provide insight into the flow behavior of the gels. K represents the consistency index, while n is the flow index, which describes whether the material exhibits shear-thinning, shear-thickening, or Newtonian behavior. For $n < 1$, fluids display shear-thinning behavior, with smaller n values indicating a more pronounced shear-thinning effect (Paxton et al., 2017; Wilson et al., 2017). Additionally, low values of both K and n are advantageous, as they allow continuous flow to be achieved with lower pressure requirements (Lewis, 2006; Liu, Bhandari, Prakash, & Zhang, 2018; Liu, Zhang, et al., 2018).

All starch gels exhibited shear-thinning behavior (n < 1), characterized by a decrease in viscosity and an increase in shear stress as the shear rate increased. As shown in Fig. 7A, the K values of all six samples generally decreased initially and then increased over time. Notably, the BP577, BL02, and BL03 samples consistently maintained lower K values compared to the LTFB, BL06, and BL10 samples, indicating superior shear-thinning behavior of starches with higher AAC. Among all samples, BL02 exhibited the lowest K value overall. In Fig. 7B, the n values for BP577, LTFB, BL03, and BL10 initially increased and then decreased, suggesting a transition towards more Newtonian behavior followed by a return to more pronounced shear-thinning behavior after 7 days. In contrast, BL02 and BL06 showed little change in their n values over time. BL02 consistently displayed the highest n values at all time points, suggesting the strongest shear-thinning behavior among all samples.

3.7. Shear recovery behavior of starch gels

Starch gels with rapid and reversible viscosity responses are highly advantageous for 3D printing, as they can be easily extruded while quickly regaining sufficient mechanical strength to support subsequent layers. Shear recovery tests were conducted at a constant temperature of 25 °C. To simulate the shear conditions encountered during the extrusion printing process, we employed the procedure described by Liu, Bhandari, Prakash, Mantihal, and Zhang (2019) to investigate the effects of various shear forces on viscosity changes.

The viscosity of all starch gels decreased at high shear rates and rapidly recovered at low shear rates as shown in the recovery test profile in Fig. S5 (Lille, Nurmela, Nordlund, Metsä-Kortelainen, & Sozer, 2018). At 1 h, LTFB, BL06, and BL10 exhibited higher viscosities than BP577, BL02, and BL03. At 1 day and 7 days,LTFB, BL06, and BL10 maintained higher viscosities compared to the others, but overall, the viscosity decreased across all samples compared to 1 h. The higher viscosity of the LTFB, BL06, and BL10 at all retrogradation times indicated that these samples formed a more continuous and deformation-resistant gel network under low shear (Cheng et al., 2024). This feature is likely contributed to their lower amylose contents, as amylopectin chains are longer or more entangled, they can further increase paste viscosity (Juhász & Salgó, 2008). The recovery ability in Fig. 8 displayed similar trend: LTFB, BL06, and BL10 exhibited higher shear recoverability than other three samples at the same retrogradation time, with shear recoverability reduced at 1 day and 7 days compared to 1 h.

3.8. Rheological properties of starch gels

Rheological properties (Fig. 9) are essential characteristics of starch gels, with key parameters including the storage (elastic) modulus (G′), loss (viscous) modulus (G″), complex modulus (G*), and loss angle tangent (Tan δ = G″/G′) (Chen et al., 2022). The storage modulus (G′) was consistently higher than the viscous modulus (G″), and both exhibited frequency-dependent behavior (Fig. 9A and B). Tan δ serves as an indicator of whether the material behaves more like a solid (elastic) or a fluid (viscous); when Tan δ < 1 (Fig. 9D), the material demonstrates greater elasticity than viscosity. Both G′ and G* are critical for the self-supporting ability of the gel and for maintaining the integrity of

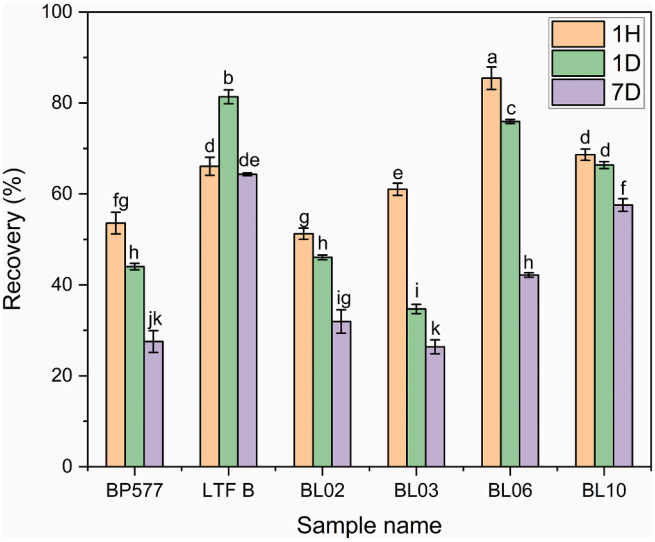


Fig. 8. Shear recoverability of different starch hydrogels retrograded for 1 h, 1 day, and 7 days determined as the percentage of viscosity obtained during the first 30s in the third step based on the average viscosity obtained in the first step.

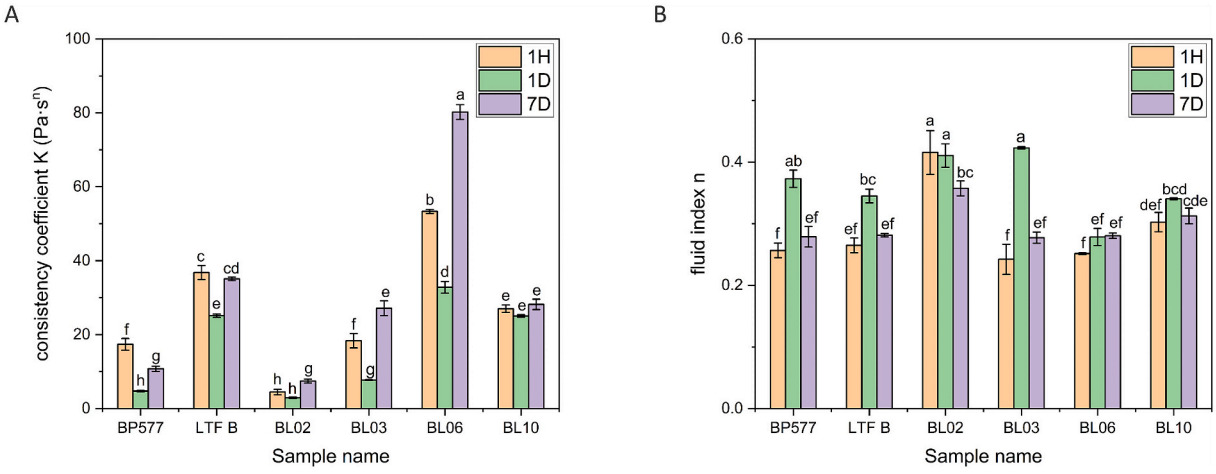


Fig. 7. Consistency index (K) and flow index (n) of different starch hydrogels retrograded for 1 h, 1 day, and 7 days. (A) Consistency index (K). (B) Flow index (n).

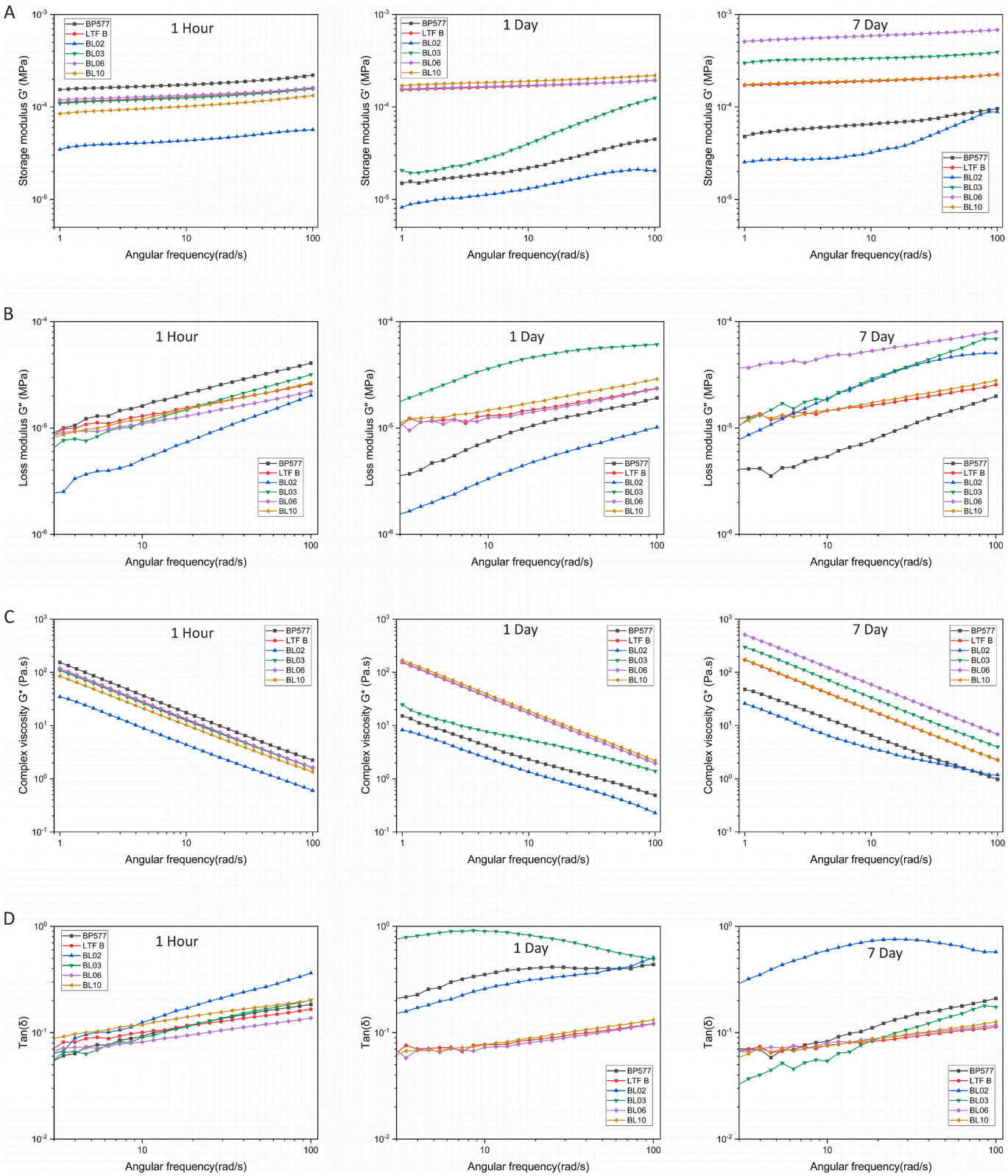


Fig. 9. Rheological properties of different starch hydrogels retrograded for 1 h, 1 day, and 7 days. (A) Storage modulus (G′). (B) Loss modulus (G″). (C) Complex modulus (G*). (D) Tan δ, the tangent of the phase angle between G′ and G″.

deposited structures (Huang, 2018; Lille et al., 2018).

As shown in Fig. 9A, after 1 h of retrogradation, differences in G′ and G* among all samples were minimal, except for BL02, which exhibited significantly lower values than others. However, after 1 day of retrogradation, the G′ and G* values of BP577, BL02, and BL03 with higher amylose contents were significantly lower than those of samples with lower amylose contents (Fig. 9A and C). This suggests that lower amylose content enhanced the resistance to deformation after 1 day of retrogradation, possibly due to the higher recovery capability of starch printing pastes. After 7 days of retrogradation, the G′ and G* values of

BL03 and BL06 increased significantly, surpassing those of all other samples. Notably, BL06 formed a denser gel network during the later stages of retrogradation, attributed to its higher content of long branches, resulting in stronger resistance to deformation. However, as retrogradation progressed to the 7 days, the Tan δ of the printing paste continued to decrease, and the paste gradually adopted a jelly-like consistency. In rheological tests, this may not accurately reflect its true viscoelasticity and resistance to deformation. Nevertheless, these measurements still provide valuable information regarding the self-supporting behavior of the deposited object after the ink reaches a stable state and during subsequent storage.

3.9. Printing performance of starch printing pastes

To assess the printing performance of starch printing pastes, a relatively complex pattern was selected, as its successful fabrication required precise handling of numerous details and superior printing performance to achieve high-quality results. Fig. 10 presents the printing outcomes of starch gels retrograded for different durations. The 3D printing performance was evaluated according to extrusion continuity, colloid uniformity, edge definition, internal fill quality, and shape retention under identical printing conditions.

After 1 h of retrogradation, LTFB and BL10 exhibited the best initial print quality among all samples, followed by BL06, while other three starch samples had lower values, indicating that lower amylose content is associated with better initial printability. However, as retrogradation progressed, both LTFB and BL10 showed a steady decline in print quality, with noticeable decreases after 1 day. Despite this decline, their performance stabilized and were the best by day 7, indicating that these two samples maintained relatively high and consistent print quality over time. In contrast, the other four samples (BP577, BL02, BL03, and BL06) demonstrated optimal print quality after 1 day of retrogradation, with BL03 achieving the highest performance among them, reflecting enhanced structural stability and printability during 1 day of retrogradation. However, all four samples experienced a marked decline in print quality by day 7, indicating reduced long-term print stability and structural integrity.

4. Discussion

4.1. The relationships between the molecular structure of starch and the gel structure

The honeycomb-like porous structure of starch gels is formed during the freezing process, as water within the gel crystallizes into ice and displaces the starch molecular network onto the pore walls (Ahmadzadeh & Ubeyitogullari, 2023). Consequently, the network structure resulting from the aggregation of starch molecules serves as the foundation for the architecture of starch gels. Amylose aggregates into a network at a much faster rate than amylopectin (Putaux et al., 2000). Therefore, during the 1 h of retrogradation, the starch gel network is primarily composed of semi-crystalline aggregates formed by the reassociation of amylose molecules. The relative lengths between the semi-crystalline regions formed by amylose molecules are relatively large during this early retrogradation period (Fig. 3A), resulting in an incomplete dense structure, weak gel strength, and low resistance to ice crystal growth. Consequently, larger pore areas are formed in the starch gels after freeze-drying (Fig. 2A). A higher amylose content leads to the formation of more compact semi-crystalline aggregates (Fig. 3A). Therefore, samples with ultra-high amylose content rapidly form B-type crystals (Fig. 4), with smaller pore areas and lower pore fraction (Fig. 2) in the gels compared to LTFB, BL06, and BL10. As starch gels further retrograde over time, the water-rich network condenses into dense semi-crystalline aggregates. However, due to the random nature of intermolecular associations in starch and the restricted molecular mobility imposed by molecular weight and storage temperature, starch gels do not achieve high crystallinity (Putaux et al., 2000). Consequently, the semi-crystalline aggregates within the gel eventually stabilize at a certain state and cannot fully recover their crystallinity. In samples with ultra-high amylose content, the correlation lengths between semi-crystalline units (Fig. 3A) within the gel network and the area of the porous structure (Fig. 2A) stabilize after just 1 day of retrogradation, indicating a faster aggregation process and the formation of stronger B-type crystalline structure (Fig. 4B). As the amylose molecular network aggregates and condenses, gel strength increases and water is expelled from the interior of the starch gel, and more bound water is formed (Fig. 5), thereby leading to enhanced resistance to ice crystal growth and a reduction in the pore area, pore fraction and rg of the resulting starch gel after 7 days of retrogradation.

The structure and composition of amylopectin also play a crucial role in the formation and retrogradation of starch gels (Bertoft et al., 2016). Amylopectin features inner chains that form internal helical segments, and possesses outer chains that interact with neighboring molecules within the gel (Bertoft et al., 2016). Although the number of these interactions is relatively small, both amylopectin-amylopectin and amylose-amylopectin interactions contribute to the changes observed in the gel during long-term storage (Klucinec & Thompson, 1999). Despite the decrease in the correlation length of semi-crystalline aggregates within the starch gel network structure during retrogradation, the size of the aggregates themselves exhibits a different trend (Fig. 3B). It is speculated that this may be due to the formation of double-helical interconnections between amylopectin molecules and between amylopectin and amylose molecules in the later stages of retrogradation, leading to the formation of new aggregates. Under similar amylose content conditions, gels formed by amylopectin with more long chains (BL06) and those with shorter average chain lengths (LTFB and BL10) show significant differences during retrogradation. When the starch gel contains more long chains, the retrogradation effect is more

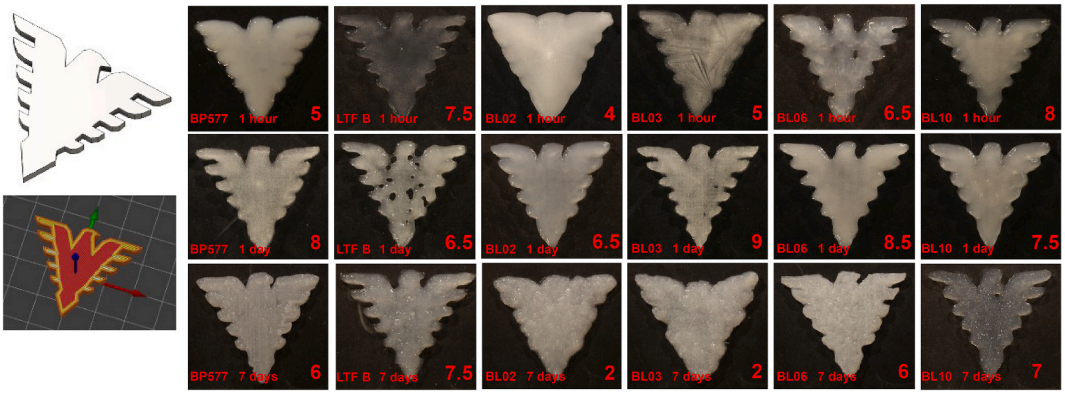


Fig. 10. 3D Printing performance of different rice starch hydrogels retrograded for 1 h, 1 day, and 7 days.

pronounced, resulting in a noticeable compactness of starch gel structure, lower pore area (Fig. 2A) and correlation length between crystalline aggregates (Fig. 3B), but higher B-type crystals within the gel (Fig. 4B and C). These indicated that the longer chains of amylopectin have a more significant impact on gel formation, which is consistent with the findings of Bertoft et al. (2016). This may be attributed to the fact that intermolecular interactions primarily occur between the longer internal chain segments and the outer chains of amylopectin molecules, either forming double helices between the outer chains of two molecules or composites constituted by two double helices formed by the outer chains of adjacent molecules (Klucinec & Thompson, 1999; Shen, Bertoft, Zhang, & Hamaker, 2013).

In addition, the proportion of free water in starch gels exhibits a significant positive correlation with the pore structure of the gels and the structural radii of the aggregates (Fig. S6), whereas the proportion of bound water and the mobility of water molecules show a negative correlation with the gel pore structure and the size of semi-crystalline aggregates. This suggests that dense gel networks formed during the later stages of retrogradation in gels containing more amylose and long-chain amylopectin exhibit increased syneresis (dehydration contraction), while amylopectin with shorter average chain lengths demonstrates better water retention capacity.

Our results partly agree with previous studies showing that increased amylose generally promotes molecular reassociation and retrogradation (Lii, Tsai, & Tseng, 1996), but differ from studies in which higher amylose led to higher yield stress or greater gel rigidity (Yu, Ma, & Sun, 2009). This discrepancy likely arises because printability is not determined by amylose content alone. In the present rice starch system, excessive amylose accelerated the formation of dense semi-crystalline regions and water redistribution during storage, which may have promoted local brittleness, microstructural heterogeneity, and reduced post-shear structural recovery. Thus, although amylose-rich samples retrograded faster, they did not maintain the most favorable balance between extrusion and deposition stability over prolonged storage.

4.2. The relationship between the molecular structure of starch and printability in 3D food printing

During the retrogradation process, samples with ultra-high amylose content exhibit lower yield stress, consistency coefficient, recovery ability, and viscoelasticity in terms of their rheological properties. In previous studies, systems with higher amylose content were found to possess more compact structures, resulting in higher elastic moduli and yield stresses (Cheng et al., 2024; Obadi, Qi, & Xu, 2023; Xiao et al., 2021), which is inconsistent with our findings. It is speculated that the ratio of amylose to amylopectin, as well as their molecular structures, significantly influence the association of starch chains and structural properties (Cheng et al., 2024; Schirmer, Höchstötter, Jekle, Arendt, & Becker, 2013). Therefore, it is inaccurate to solely judge the impact on gel properties based on amylose content alone. The rheological properties of the material are related to the formation of intermolecular double helices within starch gels. And the proportion of double-helical structures in starch gels increases with higher amylose content (Fang, Martinez, Campanella, & Hamaker, 2020). However, when the amylose content is excessively high (ultra-high amylose content), the density of double-helical structures within the gel increases, leading to the rapid formation of crystalline regions (Fig. 4). This further results in an overly rigid network structure that lacks toughness. Such a brittle structure is prone to fracture under stress rather than undergoing elastic deformation, thereby reducing the yield stress and elastic modulus. Additionally, the ratio of amylose to amylopectin affects water distribution, with higher amylose content leading to a reduction in free water within the gel (Fig. 5) and the occurrence of syneresis. This shrinkage induces microcracks within the gel, disrupting the integrity of the network and subsequently reducing elasticity and resistance to deformation.

Compared to samples with ultra-high amylose content, LTFB, BL06, and BL10 exhibit higher yield stress, consistency coefficient, recovery ability, and viscoelasticity. The BL06, which contains more long-branched chains, demonstrated the highest values for these gel properties. This might be attributed to the synergistic effect between amylose and amylopectin. Amylopectin, through its branched structure, provides more cross-linking points, enhancing the network's elasticity and promoting mutual adhesion within the gel (Xing et al., 2023). Amylose forms crystalline regions during the gel formation process, reinforcing the rigidity, while amylopectin, due to its high degree of branching, increases the cross-linking density, thereby improving the continuity of the gel network. Under external stress, the gel can distribute the force evenly through its chain segments, enhancing the overall structural toughness. BL06, with its abundance of long-branched chains, enables the formation of more double-helical structures via its outer chains, further enhancing the resistance to deformation of the gel compared to LTFB and BL10.

After 1 day of retrogradation, the starch gels of all samples became structurally denser, with further reductions in yield stress, consistency coefficient, and recoverability, while the viscosity index increased. After 7 days of retrogradation, the yield stress and consistency coefficient of the starch gels rebounded, whereas the viscosity index decreased. This indicates that the starch gel network becomes overly rigid in the later stages of retrogradation, making it less suitable for use as a printing paste. Notably, among samples with lower amylose content, BL06, which possesses more long-branched chains, exhibited a structure similar to that of high-amylose samples after 7 days of retrogradation. However, unlike other high-amylose samples, BL06 demonstrated higher yield stress, consistency coefficient, recovery ability, and resistance to deformation. This may be attributed to the fact that, during retrogradation, long-branched amylopectin primarily undergoes intramolecular interactions. The primary structure of amylopectin facilitates the formation of double helices through the interlocking of small side chains (Putaux et al., 2000). Additionally, the intermolecular connections formed by the long chains of amylopectin extend and create new cross-links with prolonged retrogradation time (Bertoft et al., 2016). These double helices combine with amylose molecules and other amylopectin molecules to form larger semi-crystalline aggregates. The structural characteristics of clusters within these semi-crystalline aggregates and the shorter inter-crystalline segments contribute to the higher mechanical strength of the gel structure.

Despite its higher rigidity, BL06 exhibits lower shear recovery compared to LTFB and BL10 after 7 days of retrogradation, highlighting the trade-off between structural strength and printability. This trade-off is critical in 3D starch printing, as retrogradation determines long-term performance (Wang, Li, Copeland, Niu, & Wang, 2015). Clarifying amylopectin fine structure's impact on retrogradation is key to optimizing starch for 3D printing. The CLD of amylopectin significantly influences retrogradation. Chains with DP 24–36 and DP $\geq$36 promote ordered crystallization, while chains with DP 6–12 inhibit this process (Li et al., 2021). BL06, with longer chains, has a higher fb1 content and lower fa content, leading to reduced shear recovery and flexibility. In contrast, LTFB and BL10, both carrying the SSIIa-TT allele, contained a higher proportion of fa chains and a higher fa/fb1 balance, which likely improved chain mobility and delayed excessive ordering during storage. This behavior is consistent with reports that shorter amylopectin chains can suppress or delay extensive long-range ordering while helping maintain water retention and viscoelastic recovery (Li et al., 2021). Our data therefore suggest that the most favorable starch for long-term 3D printing is not the one with the highest retrogradation tendency, but the one that maintains a better compromise between structural support and shear-induced rebuild ability. For 3D printing materials, flowability and stability are two crucial key points. Yield stress and consistency coefficient are more closely related to flowability, whereas shear recovery, viscoelasticity, and moderate structural strength are more important for post-deposition stabilization. Taken together, the results support a

multi-level structure–property–printability relationship. At the molecular level, higher amylose content accelerated retrogradation and promoted denser semi-crystalline aggregation, while differences in amylopectin fine structure further modulated water retention and network rebuild ability. At the gel-structure level, reduced pore area, smaller rg, and increased bound-water characteristics reflected network densification during storage. At the rheological level, lower yield stress and lower K favored extrusion, whereas higher recovery and moderate Tan δ were more important for post-deposition stabilization. Therefore, optimal printability required not only easy flow through the nozzle but also sufficient structural recovery after extrusion, which explains why the best-performing samples differed between 1 day and 7 days of retrogradation.

4.3. Genetic modification of starch to modulate amylopectin structure and enhance 3D printability

Previous studies have reported the significance of rheological properties such as yield stress, shear-thinning behavior, viscosity, and shear recovery ability in determining the 3D printability of starch-based materials. These properties are critical for both the extrusion and recovery phases during the 3D printing process. Starches with low viscosity and yield stress are easier to extrude, while those exhibiting shear-thinning behavior and dynamic viscoelasticity can form continuous filaments and recover their structure after extrusion. The fine molecular structure of amylopectin plays a key role in shaping these rheological properties, directly influencing starch printability.

In this study, we explored genetic modification as an alternative to traditional post-harvest modification methods, which often require multiple processing steps. Genetic modification, particularly through molecular marker-assisted crossbreeding, directly alters starch biosynthesis pathways, offering a more efficient, sustainable, and precise approach to controlling starch structure. By targeting key genes such as *BEIIb* and *SSIIa*, we modulated amylose content and amylopectin chain length, significantly impacting the rheological and printing characteristics of the starch gel. Among the six rice starches studied, those lacking BEIIb (BP577, BL02, BL03) exhibited extremely high amylose contents (>30%), which promoted rapid formation of dense semi-crystalline regions and resulted in higher storage modulus (G′) with low yield stress and consistency coefficients. However, these gels showed poor recovery after shear and significant syneresis during prolonged retrogradation, leading to inferior printability after 7 days of retrogradation. In contrast, starches from LTFB, BL06, and BL10, which retained functional *BEIIb* expression and had moderate amylose levels (26–29%), displayed more balanced rheological profiles and better printability across all retrogradation times. Subtle differences were observed among these three starch samples, particularly in their performance after 7 days of retrogradation. BL06, which carries the SSIIaGC allele, exhibited slightly inferior long-term printability compared to LTFB and BL10 (SSIIaTT).

This approach aligns with recent advances in starch modification for 3D food printing (Rong et al., 2023). Physical processing techniques, such as high-pressure processing (HPP) and microwave heating, are commonly used to modify starch and improve its rheological properties. These methods are effective in altering the microstructure of starch, increasing gel strength, and enhancing printability (Castro, Alexandre, Saraiva, & Pintado, 2020). However, they require additional processing steps and can lead to inconsistent results, particularly regarding gel recovery and long-term printability (Koshenaj & Ferrari, 2024; Larrea-Wachtendorff, Sousa, & Ferrari, 2021). Chemical modifications, such as esterification or oxidation, can also improve starch flow behavior but often negatively affect texture, flavor, and nutritional quality, limiting their applicability in food products (Chaudhary, Miler, Torley, Sopade, & Halley, 2008; Masina et al., 2016). In contrast, genetic modification offers a more precise approach by directly targeting genetic factors that govern the amylose/amylopectin balance and other structural characteristics. This makes genetic modification a more sustainable and cost-effective solution for optimizing starch for 3D printing. From an industrial perspective, the feasibility of this approach depends on the route used to generate the starch source material. In the present study, the rice lines were developed through molecular marker-assisted crossbreeding rather than post-harvest chemical modification, which may improve practical acceptability in food applications and provide a promising route for developing starches with more predictable 3D printing functionality.

5. Conclusion

The effects of genetic modifications on starch gel properties relevant to 3D printing were investigated using six rice starches with varying amylose contents (26.85%–33.84%) and distinct amylopectin structures. *BEIIb* knockout lines (BP577, BL02, BL03) produced high-amylose starches, characterized by higher storage modulus and crystallinity and lower shear recovery and stability during prolonged retrogradation, thereby leading to the best mid-term printability (1 day) but low initial (1 h) and long-term (7 days) printability. In contrast, starches with intact *BEIIb* (LTFB, BL06, BL10) demonstrated improved viscoelastic recovery and shape retention after 7 days of retrogradation. Furthermore, $SSIIa^{TT}$ (LTFB, BL10) increased the proportion of fa chains in amylopectin, resulting in lower Tan δ values, more stable K values, and enhanced initial and long-term printability. Conversely, $SSIIa^{GC}$ (BL06) promoted the formation of fb1 chains, reduced fa content, and weakened gel flexibility, presenting good mid-term printability. These findings provide new evidence that the fa/fb1 balance plays a critical role in modulating the printability of starch gels, highlighting the potential of molecular breeding to optimize amylopectin structure for 3D food printing applications. However, the underlying mechanisms by how chain rearrangement influences long-term printability remain unclear and warrant further investigation across diverse starch types and genetic backgrounds.

CRediT authorship contribution statement

Yaqi Hu: Writing – review & editing, Writing – original draft, Software, Methodology, Investigation, Conceptualization. **Ziliang Qin:** Writing – review & editing, Writing – original draft, Software, Methodology, Investigation. **Li Ding:** Writing – review & editing. **Xiaoning Liu:** Writing – review & editing. **Xingxun Liu:** Software, Methodology, Conceptualization. **Deyong Zhu:** Software, Methodology, Conceptualization. **Jacob Judas Kain Kirkensgaard:** Formal analysis. **Tomasz Pawel Czaja:** Writing – review & editing, Writing – original draft, Supervision. **Sheng Chen:** Writing – review & editing, Writing – original draft, Supervision. **Andreas Blennow:** Writing – review & editing, Writing – original draft, Supervision. **Jiyu Yang:** Writing – review & editing, Writing – original draft. **Jinsong Bao:** Writing – review & editing, Supervision, Resources, Funding acquisition, Conceptualization. **Yuyue Zhong:** Writing – review & editing, Supervision, Resources, Funding acquisition, Conceptualization.

Declaration of competing interest

The authors declare that they have no known competing financial interests or personal relationships that could have appeared to influence the work reported in this paper.

Acknowledgements

This work was supported by the Hainan Provincial Natural Science Foundation of China (326ZD1002) and National Natural Science Foundation of China (Grant 32372476). The WAXS and SAXS data were generated via a research infrastructure at the University of Copenhagen, partly funded by FOODHAY (Food and Health Open Innovation Laboratory, Danish Roadmap for Research Infrastructure).

Appendix A. Supplementary data

Supplementary data to this article can be found online at https://doi.org/10.1016/j.foodchem.2026.150774.

Data availability

Data will be made available on request.

References

Achayuthakan, P., & Suphantharika, M. (2008). Pasting and rheological properties of waxy corn starch as affected by guar gum and xanthan gum. *Carbohydrate Polymers, 71*(1), 9–17.

Ahmadzadeh, S., & Ubeyitogullari, A. (2023). Generation of porous starch beads via a 3D food printer: The effects of amylose content and drying technique. *Carbohydrate Polymers, 301*, Article 120296.

Bao, J., Shen, S., Sun, M., & Corke, H. (2006). Analysis of genotypic diversity in the starch physicochemical properties of nonwaxy rice: Apparent amylose content, pasting viscosity and gel texture. *Starch - Stärke, 58*(6), 259–267.

Bertoft, E., Annor, G. A., Shen, X., Rumpagaporn, P., Seetharaman, K., & Hamaker, B. R. (2016). Small differences in amylopectin fine structure may explain large functional differences of starch. *Carbohydrate Polymers, 140*, 113–121.

Bhardwaj, R., & Saini, C. S. (2025). Functional, pasting, rheological, crystalline, and thermal properties of red rice starch from northern Indian sub-Himalayan belt: A comparative study with basmati rice. *Bioactive Carbohydrates and Dietary Fibre*, Article 100515.

Castro, L. M., Alexandre, E. M., Saraiva, J. A., & Pintado, M. (2020). Impact of high pressure on starch properties: A review. *Food Hydrocolloids, 106*, Article 105877.

Chaudhary, A. L., Miler, M., Torley, P. J., Sopade, P. A., & Halley, P. J. (2008). Amylose content and chemical modification effects on the extrusion of thermoplastic starch from maize. *Carbohydrate Polymers, 74*(4), 907–913.

Chen, S., Qin, L., Chen, T., Yu, Q., Chen, Y., Xiao, W., … Xie, J. (2022). Modification of starch by polysaccharides in pasting, rheology, texture and *in vitro* digestion: A review. *International Journal of Biological Macromolecules, 207*, 81–89.

Chen, Y., Zhang, M., Sun, Y., & Phuhongsung, P. (2022). Improving 3D/4D printing characteristics of natural food gels by novel additives: A review. *Food Hydrocolloids, 123*, Article 107160.

Cheng, Y., Yuqing, H., Xiao, L., Gao, W., Kang, X., Sui, J., & Cui, B. (2024). Impact of starch amylose and amylopectin on the rheological and 3D printing properties of corn starch. *International Journal of Biological Macromolecules, 278*, Article 134403.

Cisneros, F. H., Zevillanos, R., & Cisneros-Zevallos, L. (2009). Characterization of starch from two ecotypes of andean achira roots (*Canna edulis*). *Journal of Agricultural and Food Chemistry, 57*(16), 7363–7368.

Fang, F., Martinez, M. M., Campanella, O. H., & Hamaker, B. R. (2020). Long-term low shear-induced highly viscous waxy potato starch gel formed through intermolecular double helices. *Carbohydrate Polymers, 232*, Article 115815.

Fei, Y., Han, H., Yu, B., Gong, H., & Jing, D. (2023). Physicochemical properties of waxy rice varieties with contrasting hardening rates. *International Journal of Food Properties, 26*(1), 1775–1786.

Feng, C., Wang, Q., Li, H., Zhou, Q., & Meng, W. (2018). Effects of pea protein on the properties of potato starch-based 3D printing materials. *International Journal of Food Engineering, 14*(3), Article 20170297.

Gao, Q., Zhang, B., Qiu, L., Fu, X., & Huang, Q. (2020). Ordered structure of starch inclusion complex with C10 aroma molecules. *Food Hydrocolloids, 108*, Article 105969.

Gao, S., Sun, S., Zhao, J., Wang, W., & Hou, H. (2024). A biodegradable pH-response packaging film with blueberry extract: Blown-extrusion fabrication, multifunctional activity, and kinetic investigation. *Food Chemistry, 449*, Article 139217.

He, M., Qiu, C., Liao, Z., Sui, Z., & Corke, H. (2018). Impact of cooking conditions on the properties of rice: Combined temperature and cooking time. *International Journal of Biological Macromolecules, 117*, 87–94.

Hu, Y., Zhang, Y., Yu, S., Deng, G., Dai, G., & Bao, J. (2023). Combined effects of *BEIIb* and *SSIIa* alleles on amylose contents, starch fine structures and physicochemical properties of *indica* rice. *Foods, 12*(1), 119.

Hu, Y., Zhang, Z., Li, X., Yu, J., Chen, Y., & Bao, J. (2025). The functions of rice SSIIa alleles in starch biosynthesis modulated by the distinct genetic backgrounds. *Carbohydrate Polymers, 367*, Article 123987.

Huang, C. Y. (2018). *Extrusion-based 3D printing and characterization of edible materials* (Vol. Master). University of Waterloo.

Jain, S., Winuprasith, T., & Suphantharika, M. (2019). Design and synthesis of modified and resistant starch-based oil-in-water emulsions. *Food Hydrocolloids, 89*, 153–162.

Jane, J. L., & Robyt, J. F. (1984). Structure studies of amylose-V complexes and retrograded amylose by action of alpha amylases, and a new method for preparing amylodextrins. *Carbohydrate Research, 132*(1), 105–118.

Juhász, R., & Salgó, A. (2008). Pasting behavior of amylose, amylopectin and their mixtures as determined by RVA curves and first derivatives. *Starch-Stärke, 60*(2), 70–78.

Klucinec, J. D., & Thompson, D. B. (1999). Amylose and amylopectin interact in retrogradation of dispersed high-amylose starches. *Cereal Chemistry, 76*(2), 282–291.

Koshenaj, K., & Ferrari, G. (2024). Optimization of processing conditions of starch-based hydrogels produced by high-pressure processing (HPP) using response surface methodology. *Frontiers in Food Science and Technology, 4*, 1376044.

Larrea-Wachtendorff, D., Sousa, I., & Ferrari, G. (2021). Starch-based hydrogels produced by high-pressure processing (HPP): Effect of the starch source and processing time. *Food Engineering Reviews, 13*(3), 622–633.

Lewis, J. A. (2006). Direct ink writing of 3D functional materials. *Advanced Functional Materials, 16*(17), 2193–2204.

Li, C. (2024). Unraveling the complexities of starch retrogradation: Insights from kinetics, molecular interactions, and influences of food ingredients. *Food Reviews International, 40*(9), 3159–3182.

Li, C., & Gong, B. (2020). Insights into chain-length distributions of amylopectin and amylose molecules on the gelatinization property of rice starches. *International Journal of Biological Macromolecules, 155*, 721–729.

Li, C., Hu, Y., & Li, E. (2021). Effects of amylose and amylopectin chain-length distribution on the kinetics of long-term rice starch retrogradation. *Food Hydrocolloids, 111*, Article 106239.

Li, H., Liu, S., & Li, L. (2016). Rheological study on 3D printability of alginate hydrogel and effect of graphene oxide. *International Journal of Bioprinting, 2*(2), 163–175.

Li, L., Zhao, Y., Mou, A., Shen, X., Liu, Z., & Luo, Z. (2025). Influence of highland barley β-glucan on textural, structural, and rheological characteristics of corn starch. *International Journal of Biological Macromolecules, 307*, Article 141971.

Liang, Y., Wang, F., Ma, R., & Tian, Y. (2024). Structural properties of the intra- and interhelical cavities of V6-type crystalline starches. *Carbohydrate Polymers, 330*, Article 121835.

Lii, C.-Y., Tsai, M.-L., & Tseng, K.-H. (1996). Effect of amylose content on the rheological property of rice starch. *Cereal Chemistry, 73*(4), 415–420.

Lille, M., Nurmela, A., Nordlund, E., Metsä-Kortelainen, S., & Sozer, N. (2018). Applicability of protein and fiber-rich food materials in extrusion-based 3D printing. *Journal of Food Engineering, 220*, 20–27.

Lin, L., Huang, J., Zhang, L., Liu, Q., & Wei, C. (2020). Effects of inhibition of starch branching enzymes on starch ordered structure and component accumulation in developing kernels of rice. *Journal of Cereal Science, 91*, Article 102884.

Liu, J., Sun, L., Xu, W., Wang, Q., Yu, S., & Sun, J. (2019). Current advances and future perspectives of 3D printing natural-derived biopolymers. *Carbohydrate Polymers, 207*, 297–316.

Liu, Y., Tang, T., Duan, S., Qin, Z., Zhao, H., Wang, M., … Dong, Y. (2020). Applicability of rice doughs as promising food materials in extrusion-based 3D printing. *Food and Bioprocess Technology, 13*(3), 548–563.

Liu, Z., Bhandari, B., Prakash, S., Mantihal, S., & Zhang, M. (2019). Linking rheology and printability of a multicomponent gel system of carrageenan-xanthan-starch in extrusion based additive manufacturing. *Food Hydrocolloids, 87*, 413–424.

Liu, Z., Bhandari, B., Prakash, S., & Zhang, M. (2018). Creation of internal structure of mashed potato construct by 3D printing and its textural properties. *Food Research International, 111*, 534–543.

Liu, Z., Zhang, M., Bhandari, B., & Yang, C. (2018). Impact of rheological properties of mashed potatoes on 3D printing. *Journal of Food Engineering, 220*, 76–82.

Ma, S., Zhu, P., Wang, M., Wang, F., & Wang, N. (2019). Effect of konjac glucomannan with different molecular weights on physicochemical properties of corn starch. *Food Hydrocolloids, 96*, 663–670.

Masina, N., Choonara, Y. E., Kumar, P., Du Toit, L. C., Govender, M., Indermun, S., & Pillay, V. (2016). A review of the chemical modification techniques of starch. *Carbohydrate Polymers*, 1226.

Miura, S., Crofts, N., Saito, Y., Hosaka, Y., Oitome, N. F., Watanabe, T., … Fujita, N. (2018). Starch synthase IIa-deficient mutant rice line produces endosperm starch with lower gelatinization temperature than japonica rice cultivars. *Frontiers in Plant Science, 9*, 645.

Moo-Huchin, V. M., Cabrera-Sierra, M. J., Estrada-León, R. J., Ríos-Soberanis, C. R., Betancur-Ancona, D., Chel-Guerrero, L., … Pérez-Pacheco, E. (2015). Determination of some physicochemical and rheological characteristics of starch obtained from *Brosimum alicastrum* swartz seeds. *Food Hydrocolloids, 45*, 48–54.

Müller, J. J., Gernat, C., Schulz, W., Müller, E.-C., Vorwerg, W., & Damaschun, G. (1995). Computer simulations of X-ray scattering curves: Gelation and crystallization process in amylose solutions. *Biopolymers, 35*(3), 271–288.

Obadi, M., Qi, Y., & Xu, B. (2023). High-amylose maize starch: Structure, properties, modifications and industrial applications. *Carbohydrate Polymers, 299*, Article 120185.

Okpala, N. E., Aloryi, K. D., An, T., He, L., & Tang, X. (2022). The roles of starch branching enzymes and starch synthase in the biosynthesis of amylose in rice. *Journal of Cereal Science, 104*, Article 103393.

Outrequin, T. C. R., Gamonpilas, C., Siriwatwechakul, W., & Sreearunothai, P. (2023). Extrusion-based 3D printing of food biopolymers: A highlight on the important rheological parameters to reach printability. *Journal of Food Engineering, 342*, Article 111371.

Paxton, N., Smolan, W., Böck, T., Melchels, F., Groll, J., & Jungst, T. (2017). Proposal to assess printability of bioinks for extrusion-based bioprinting and evaluation of rheological properties governing bioprintability. *Biofabrication, 9*(4), Article 044107.

Punia, S., Sandhu, K. S., Dhull, S. B., & Kaur, M. (2019). Dynamic, shear and pasting behaviour of native and octenyl succinic anhydride (OSA) modified wheat starch and their utilization in preparation of edible films. *International Journal of Biological Macromolecules, 133*, 110–116.

Putaux, J.-L., Buleon, A., & Chanzy, H. (2000). Network formation in dilute amylose and amylopectin studied by TEM. *Macromolecules, 33*(17), 6416–6422.

Qin, Z., Yang, Y., Zhang, Z., Li, F., Hou, Z., Li, Z., … Shen, T. (2025). A critical review: Gel-based edible inks for 3D food printing: materials, rheology–geometry mapping, and control. *Gels, 11*(10), 780.

Rong, L., Chen, X., Shen, M., Yang, J., Qi, X., Li, Y., & Xie, J. (2023). The application of 3D printing technology on starch-based product: A review. *Trends in Food Science & Technology, 134*, 149–161.

Rong, L., Shen, M., Wen, H., Xiao, W., Li, J., & Xie, J. (2022). Effects of xanthan, guar and *Mesona chinensis* Benth gums on the pasting, rheological, texture properties and microstructure of pea starch gels. *Food Hydrocolloids, 125*, Article 107391.

Schirmer, M., Höchstötter, A., Jekle, M., Arendt, E., & Becker, T. (2013). Physicochemical and morphological characterization of different starches with variable amylose/amylopectin ratio. *Food Hydrocolloids, 32*(1), 52–63.

Shen, X., Bertoft, E., Zhang, G., & Hamaker, B. R. (2013). Iodine binding to explore the conformational state of internal chains of amylopectin. *Carbohydrate Polymers, 98*(1), 778–783.

Shi, S., Wen, J., Geng, H., Zhan, X., & Liu, Y. (2024). Physicochemical properties, structural properties and gels 3D printing properties of wheat starch. *International Journal of Biological Macromolecules, 261*, Article 129885.

Sweeney, M., Campbell, L. L., Hanson, J., Pantoya, M. L., & Christopher, G. F. (2017). Characterizing the feasibility of processing wet granular materials to improve rheology for 3D printing. *Journal of Materials Science, 52*(22), 13040–13053.

Syahariza, Z., Li, E., & Hasjim, J. (2010). Extraction and dissolution of starch from rice and sorghum grains for accurate structural analysis. *Carbohydrate Polymers, 82*(1), 14–20.

Wang, H., van den Berg, F. W., Zhang, W., Czaja, T. P., Zhang, L., Jespersen, B. M., & Lametsch, R. (2022). Differences in physicochemical properties of high-moisture extrudates prepared from soy and pea protein isolates. *Food Hydrocolloids, 128*, Article 107540.

Wang, S., Li, C., Copeland, L., Niu, Q., & Wang, S. (2015). Starch retrogradation: A comprehensive review. *Comprehensive Reviews in Food Science and Food Safety, 14*(5), 568–585.

Wani, A. A., Singh, P., Shah, M. A., Schweiggert-Weisz, U., Gul, K., & Wani, I. A. (2012). Rice starch diversity: Effects on structural, morphological, thermal, and physicochemical properties-A review. *Comprehensive Reviews in Food Science and Food Safety, 11*(5), 417–436.

Wani, A. A., Singh, P., Shah, M. A., Wani, I. A., Götz, A., Schott, M., & Zacherl, C. (2013). Physico-chemical, thermal and rheological properties of starches isolated from newly released rice cultivars grown in Indian temperate climates. *LWT-Food Science and Technology, 53*(1), 176–183.

Wilson, S. A., Cross, L. M., Peak, C. W., & Gaharwar, A. K. (2017). Shear-thinning and thermo-reversible nanoengineered inks for 3D bioprinting. *ACS Applied Materials & Interfaces, 9*(50), 43449–43458.

Xiao, W., Li, J., Shen, M., Yu, Q., Chen, Y., & Xie, J. (2022). Mesona chinensis polysaccharide accelerates the short-term retrogradation of debranched waxy corn starch. *Current Research in Food Science, 5*, 1649–1659.

Xiao, W., Shen, M., Ren, Y., Rong, L., Liu, W., Chen, X., … Xie, J. (2021). Mesona chinensis polysaccharides promote molecular crosslinking and gel formation of debranched waxy maize starch. *LWT, 148*, Article 111773.

Xing, B., Yang, X., Zou, L., Liu, J., Liang, Y., Li, M., … Qin, P. (2023). Starch chain-length distributions determine cooked foxtail millet texture and starch physicochemical properties. *Carbohydrate Polymers, 320*, Article 121240.

Yu, S., Ma, Y., & Sun, D.-W. (2009). Impact of amylose content on starch retrogradation and texture of cooked milled rice during storage. *Journal of Cereal Science, 50*(2), 139–144.

Zeeman, S. C., Kossmann, J., & Smith, A. M. (2010). Starch: Its metabolism, evolution, and biotechnological modification in plants. *Annual Review of Plant Biology, 61*, 209–234. volume 61, 2010.

Zeng, X., Chen, H., Chen, L., & Zheng, B. (2021). Insights into the relationship between structure and rheological properties of starch gels in hot-extrusion 3D printing. *Food Chemistry, 342*, Article 128362.

Zhang, X., Gao, X., Li, Z., Xu, L., Li, Y., Zhang, R., … Guo, D. (2020). The effect of amylose on kernel phenotypic characteristics, starch-related gene expression and amylose inheritance in naturally mutated high-amylose maize. *Journal of Integrative Agriculture, 19*(6), 1554–1564.